



Cite this: *RSC Adv.*, 2017, 7, 40896

# Probing the inhomogeneity and intermediates in the photosensitized degradation of rhodamine B by $\text{Ag}_3\text{PO}_4$ nanoparticles from an ensemble to a single molecule approach†

Beibei Xu, Xiaojuan Wang, Chaofeng Zhu, Xia Ran, Tianfeng Li\* and Lijun Guo \*

The photoinduced dynamics related to the degradation of a surface adsorbate by a semiconductive catalyst is critical for understanding the photocatalytic mechanism and improving the catalytic property of nanoscale materials. Herein, we report the investigation of the inhomogeneous interactions between  $\text{Ag}_3\text{PO}_4$  nanoparticles and rhodamine B (RhB), and the direct observation of the intermediates generated in the photodegradation of RhB, using ensemble-averaged as well as single-molecule time-resolved fluorescence spectroscopies. The results demonstrate the existence of electron injection from RhB into the conduction band of  $\text{Ag}_3\text{PO}_4$  and the formation of a deethylation intermediate before the subsequent degradation process. The fluorescence diversity both in lifetime and intensity fluctuation indicates an inhomogeneous interfacial interaction between the RhB molecule and  $\text{Ag}_3\text{PO}_4$  nanoparticle with surface heterogeneity. Based on the lifetime distribution, the duration time of single-molecule events and the related dynamical analysis, it was revealed that the RhB molecule adsorbed on the active site of the  $\text{Ag}_3\text{PO}_4$  nanoparticle has a higher injection efficiency and better photocatalytic activity. Moreover, the lifetime evolution derived from a subsection of the single-molecule emission trajectories proved that the electron injection occurred prior to the degradation through the attack of free radical  $\text{O}_2^{\cdot-}$ . These findings provide new insights into the heterogeneous interactions and dynamical information of the photosensitized degradation in an adsorbate/semiconductor catalyst.

Received 28th June 2017  
Accepted 7th August 2017

DOI: 10.1039/c7ra07163a

rsc.li/rsc-advances

## Introduction

Photocatalytic and solar energy conversion nanoscale materials and their applications, such as in the degradation of organic compounds,<sup>1–3</sup> hydrogen production by water photolysis,<sup>4</sup> and dye-sensitized solar cells (DSSCs),<sup>5</sup> have attracted much attention in the past decades. The efficiency of photocatalysis and optical energy conversion in semiconductor nanoscale photocatalysts is often affected by various parameters, including the particle size, crystalline phase, lattice or surface defects, surface area, and morphology of the particles.<sup>6</sup> The complex interactions between nanostructures and their surface adsorbates play critical roles both in photocatalytic and photosensitizing processes, since these interactions greatly affect the separation efficiency of electron–hole pairs, the generation rate of free radicals, and the injection path of electrons.<sup>7–9</sup> Further understanding of such complex dynamical interactions between nanoparticles and adsorbates would be of great significance for

designing novel materials, improving material properties, and elucidating the fundamental mechanisms of photocatalysis and pollutant degradation.

To date, considerable research efforts have been devoted to examining the pathway and mechanism of photocatalytically degrading organics by various nanoscale semiconductors to promote the separation of electron–hole pairs and therefore to enhance the photocatalytic efficiency. Rhodamine B (RhB) has often been employed as a model molecule in characterizing the degradation effect. However, the degradation process of RhB and the generated intermediate products have been investigated mostly based on ensemble-averaged methods. It has been proposed that the active sites on a catalyst surface could serve as strong electron-trapping sites to enhance the photocatalytic efficiency. Specifically, the defect sites at surfaces or interfaces of  $\text{TiO}_2$  films have been found to promote the separation of photogenerated electron–hole pairs and therefore affect the photoactivity of defective  $\text{TiO}_2$  films.<sup>10,11</sup> In another case where complexes were formed by a nanoparticle and adsorbate, it was found that the inhomogeneous interaction between a dye molecule and semiconductor surface also strongly affects the interfacial electron transfer (IET) and thus the sensitized efficiency in dye-sensitized solar cell (DSSC) systems, which have

School of Physics and Electronics, Henan University, Kaifeng 475004, P. R. China.  
E-mail: litianfeng@henu.edu.cn; juneguo@henu.edu.cn

† Electronic supplementary information (ESI) available. See DOI: 10.1039/c7ra07163a



been investigated using ultrafast spectroscopy and ensemble-averaged approaches.<sup>12,13</sup> Nevertheless, there remains an urgent need for a deeper understanding of the detailed interactions occurring on a nanoparticle surface. However, because these chemical reactions take place on heterogeneous surfaces, the spatial and temporal inhomogeneities are hard to identify and analyze using ensemble experiments. Single-molecule, single-particle fluorescence and single molecule fluorescence lifetime imaging microscopy (FLIM) have been proved to be the very powerful tools for investigating heterogeneous processes because of their high sensitivity and selectivity, simplicity of data collection, and high spatial and temporal resolution.<sup>14–18</sup> Indeed, Majima and coworkers used single-molecule dynamical observations and proposed that the reaction sites in the effective reduction of probe molecules are located on the facets with a higher surface energy.<sup>19</sup> The IET processes between a single dye molecule and TiO<sub>2</sub> nanoparticle surface demonstrate an inhomogeneity and sensitizing efficiency.<sup>20,21</sup> Compared with intensity imaging, fluorescence lifetime imaging is less susceptible to artifacts arising from scattered light, photobleaching, or non-uniform illumination of the sample, and it can thus provide an accurate approach to probing the molecular interaction changes, molecular and IET dynamics, and reaction intermediate states<sup>22–25</sup> in photocatalysis at a single molecule level.

Ag<sub>3</sub>PO<sub>4</sub> nanoparticles represent a novel photocatalyst with a band gap of 2.45 eV, which makes them a promising photocatalyst for degrading pollutants under visible light irradiation. Meanwhile, the energy of the conduction band ( $E_{CB}$ ) in Ag<sub>3</sub>PO<sub>4</sub> is fairly low to be able to accept the photoexcited electrons of adsorbed molecules, when the lowest unoccupied molecular orbital (LUMO) of the adsorbate is higher than the  $E_{CB}$ .<sup>26</sup> Ge and coworker reported that the photodegradation of methyl orange over Ag<sub>3</sub>PO<sub>4</sub> catalyst was greatly enhanced in the presence of RhB because of the injected electrons from the RhB molecule to the catalysts.<sup>27</sup> In this work, we choose the RhB–Ag<sub>3</sub>PO<sub>4</sub> nanoparticle system as a model to systematically investigate the heterogeneous catalysis and dynamical interaction between RhB and Ag<sub>3</sub>PO<sub>4</sub> nanoparticles, and particularly to probe the generation of intermediate products in the photodegradation by using ensemble-averaged spectroscopy and single-molecule fluorescence lifetime microscopy.

## Experimental

### Materials and sample preparation

Silver acetate (CH<sub>3</sub>COOAg, >99%) was purchased from Aladdin, and disodium hydrogen phosphate (Na<sub>2</sub>HPO<sub>4</sub>·12H<sub>2</sub>O, >99%) was purchased from Kermel. All of the other reagents were commercially obtained and used without further purification. Deionized water from a Milli-Q system was used in the preparation of materials. All the cover glasses (Fisher, 18 mm × 18 mm, thickness ~ 170 μm) were thoroughly cleaned by sonication in deionized water, ethanol, acetone, and deionized water, respectively for 20 min, and then dried using nitrogen gas before use. The Ag<sub>3</sub>PO<sub>4</sub> crystals were synthesized by a simple precipitation process. Briefly, CH<sub>3</sub>COOAg (200 mg) was

dissolved in 100 mL aqueous solution. Na<sub>2</sub>HPO<sub>4</sub> aqueous solution (0.15 M) was added drop by drop to the above solution with a magnetic stirrer, which was then continuously stirred for 4 h to form a golden yellow precipitation. The obtained products were repeatedly washed with deionized water to remove the remaining CH<sub>3</sub>COO<sup>−</sup> and then dried in an oven at 50 °C for 6 h.<sup>28</sup> The samples for the single-molecule experiments were prepared according to the previous literature.<sup>20</sup> For a control experiment, 25 μL of 0.05 nM solution of RhB was spin-coated onto a coverslip at 3000 rpm. The sample of RhB on Ag<sub>3</sub>PO<sub>4</sub> particles was prepared by first spin-coating 25 μL Ag<sub>3</sub>PO<sub>4</sub> dispersed solution on a clean coverslip at 2000 rpm, followed by overlaying 25 μL of 0.05 nM RhB solution onto the above coverslip.

### Characterization

The morphology of the as-prepared photocatalysts was characterized by field emission scanning electron microscopy (SEM JSM-6700F, Hitachi). The UV-Vis absorption spectra of the solid materials were recorded using a Cary 5000 UV-Vis-NIR spectrophotometer equipped with an integrating sphere attachment. The absorption spectrum of the resulting solution after photocatalysis was obtained using a PerkinElmer Lambda 35 spectrometer. The fluorescence emission spectrum was recorded at room temperature with excitation at 488 nm on a PerkinElmer fluorescence spectrometer LS55.

### Photocatalytic activity measurements

The photocatalytic activity of Ag<sub>3</sub>PO<sub>4</sub> nanoparticles was characterized by the de-colorization of RhB solution. The optical system for the photocatalytic reaction comprised a 250 W Xe lamp and a cutoff filter ( $\lambda > 400$  nm, NBeT Beijing). In the photocatalytic experiments, 15 mg of Ag<sub>3</sub>PO<sub>4</sub> nanoparticles was dispersed in RhB (100 mL, 10<sup>−5</sup> M) aqueous solution and then stirred in the dark for 30 min to reach an absorption–desorption equilibrium of RhB on the surface of Ag<sub>3</sub>PO<sub>4</sub> nanoparticles. With visible light irradiation, 2.5 mL of reaction solution was taken out at a given time. After centrifugation (10 000 rpm, 5 min), the supernatants were analyzed by monitoring the absorption maximum with a Lambda 35 UV-Vis spectrophotometer.

### Ensemble-averaged fluorescence lifetime measurements

Ensemble fluorescence decay traces were recorded using the time-correlated single photon counting (TCSPC) method with a home-built fluorescence lifetime setup (Harp300, Picoquant). A broadband tunable pulse femtosecond Ti:sapphire laser (Chameleon Ultra II, Coherent Inc.) equipped with a pulse selection system (Conoptics, Model 305) was used to obtain the excitation repetition frequency of 40 MHz. The 488 nm femtosecond excitation source was generated from the second harmonic generation with a BBO nonlinear crystal. The lens-focused fluorescence emission was separated into two channels by a dichroic mirror (ZT532rde) and passed through a band-pass filter (ET540/30 m, Chroma) and a long-pass filter (AT575lp, Chroma). The photons from different channels were



detected by two micro photon devices (MPD, Picoquant) and delivered into a TCSPC system for analysis.

### Single-molecule fluorescence lifetime measurements and imaging

Single-molecule fluorescence images were recorded on an inverted scanning confocal microscope (IX-73, Olympus) equipped with a 100 $\times$  oil immersion objective (1.4 NA, Olympus) and a close-loop nanoscale-precision piezoelectric scanning stage (Physik Instrument). A pulsed excitation source of 488 nm was generated with a BBO crystal as described previously, and the excitation pulse energy at the sample was set below 0.25 pJ. The laser beam was reflected by a dichroic beam splitter (ZT488rdc) and was focused to 100 $\times$  objective on the sample. The fluorescence was collected with the same objective, passed through a long-pass filter (ET525lp, Chroma), and focused on an MPD detector (100  $\times$  100  $\mu\text{m}^2$ ). Synchronization of the data acquisition with the scanner movement was controlled by SymPhoTime software using the time-tagged time-resolved (TTTR) measurement mode, in which each photon image was recorded by a raster scanning an area of 20  $\times$  20  $\mu\text{m}^2$  with a resolution of 128  $\times$  128 pixels.

## Results and discussion

### Ensemble-averaged observations of photodegradation

Fig. 1 shows the SEM image and absorption spectrum of the as-prepared  $\text{Ag}_3\text{PO}_4$  nanoparticles with an average diameter of about 300 nm. The crystal structure and purity of these nanoscale catalysts were further characterized by their XRD and XPS spectra (Fig. S1 and S2 $^\dagger$ ), which are consistent with the reported results in the literature.<sup>27</sup> The UV-Vis absorption spectrum indicates the particles can absorb solar light with a wavelength shorter than 520 nm (Fig. 1b). The band gap  $E_g$  of the  $\text{Ag}_3\text{PO}_4$  nanoparticle was determined to be 2.30 eV according to the equation:  $\alpha h\nu = A(h\nu - E_g)^{n/2}$ , where  $\alpha$ ,  $\nu$ , and  $A$  are the absorption coefficient, light frequency, and proportionality constant, respectively.

The photocatalytic characterization of  $\text{Ag}_3\text{PO}_4$  nanoparticles was monitored by observing the temporal changes of the maximum absorption of RhB under visible light irradiation (Fig. 2a). After 45 min, the absorption band at 554 nm was rapidly decreased and simultaneously broadened, which is similar to observations reported in the  $\text{TiO}_2/\text{RhB}$  system.<sup>10,29–31</sup>

Concomitantly, the absorption maximum of the degraded solution exhibited a slight blue-shift from 554 nm to 530 nm. This blue-shift of the absorption band could be attributed to the typical process of the photochemical deethylation of RhB from the attack of active oxygen species on the *N*-ethyl group. In the first 35 min of visible irradiation, the absorption maximum continuously decreased with the ongoing photocatalysis of  $\text{Ag}_3\text{PO}_4$  nanoparticles, due to the generated deethylated intermediates and degraded RhB. In the subsequent irradiation duration, the absorbance decreased continuously but the position of the absorption maximum no long shifted, manifesting that the intermediates were further degraded afterwards (inset of Fig. 2a). Correspondingly, the generation of intermediates in the photocatalytic process was also observed from the evolution of the fluorescence spectra of RhB degraded by  $\text{Ag}_3\text{PO}_4$  nanoparticles under visible light irradiation (Fig. 2b). We found that the emission maximum of RhB at 575 nm decreased and a new band around 535 nm appeared as the reaction proceeded, confirming the generation of the deethylated intermediate. Consistently, the fluorescence intensity of the produced intermediates increased in the first 35 min and then decreased with further irradiation, similar to the above observations in the absorption spectroscopy.<sup>29,30</sup>

To further identify the deethylation intermediates produced in the photocatalysis, we performed fluorescence lifetime measurements by monitoring the emissions of RhB and the intermediates, using a resemble-averaged two-channel TCSPC setup with tens of picosecond resolution. Briefly, the collected fluorescence signals from the photocatalytic solution were separated into two paths by a 532 nm dichroic mirror (ZT532rdc) and passed through a long-pass filter (AT575lp) for RhB and a band-pass filter (ET540/30 nm) for the deethylation intermediate, then detected by two MPDs, respectively. As shown in Fig. 2c, the decay curves of RhB ( $\lambda_{\text{em}} > 575$  nm) demonstrate little change before and after the photocatalytic reaction (not shown). However, the emission transient traces of the deethylation intermediates ( $525 \text{ nm} < \lambda_{\text{em}} < 555$  nm) exhibit an obvious evolution with the photocatalysis because the intermediate has a longer fluorescence lifetime. In fact, the photons emitted from RhB in the shorter wavelength region can be also detected by the channel of  $525 \text{ nm} < \lambda_{\text{em}} < 555$  nm, so the decay curves in this shorter wavelength region demonstrate a two-component exponential feature, where the ratio of these two components depends on the ongoing photocatalysis process. Consequently, the fluorescence lifetime ( $\tau_1$ ) of RhB in aqueous solution was determined to be 1.75 ns, while a 3.85 ns lifetime ( $\tau_2$ ) of the deethylation intermediate was obtained by fitting the trace after 55 min irradiation<sup>32,33</sup> (Fig. 2d). According to  $I(t) = A_1 \exp(-t/\tau_1) + A_2 \exp(-t/\tau_2)$ , we obtained the ratio of the two lifetime components varying with the irradiation time, and summarized the results in Table 1. These parameters clearly demonstrate that the amount of reactant RhB decreases while the produced intermediate with a longer lifetime increases as the irradiation time goes on. Therefore, this shows that the fluorescence quenching behavior with visible light irradiation originates from the degradation of RhB and the formation of deethylation intermediate.

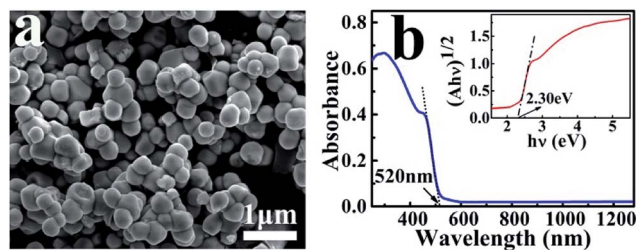


Fig. 1 SEM image (a) and UV-Vis absorption spectrum (b) of the as-prepared  $\text{Ag}_3\text{PO}_4$  nanoparticles. The inset is the plot of  $(\alpha h\nu)^{1/2}$  versus  $(h\nu)$  for the  $\text{Ag}_3\text{PO}_4$  to derive the band gap.





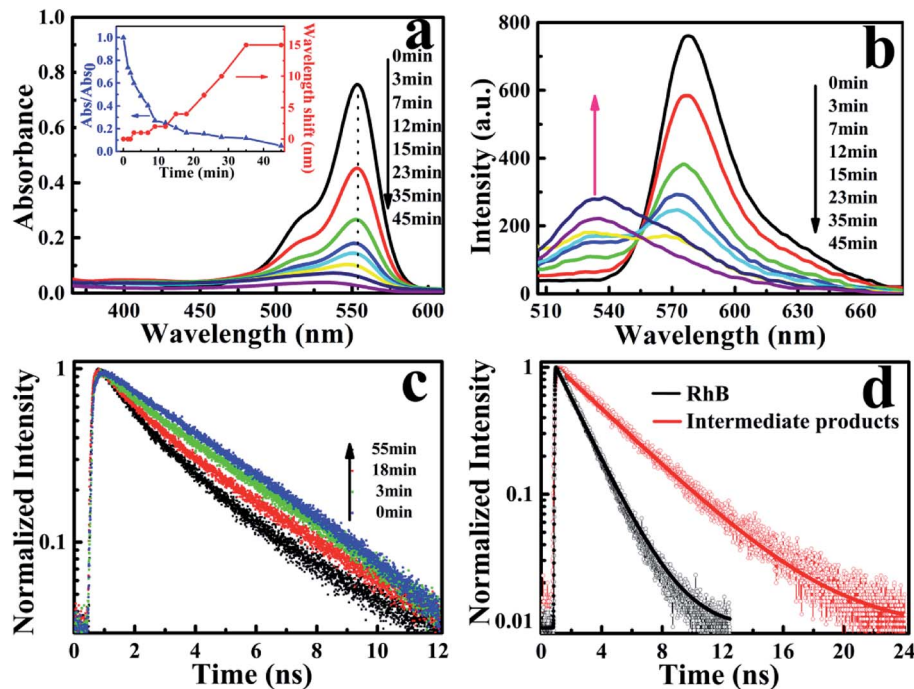


Fig. 2 (a) UV-Vis spectral changes with visible irradiation time in the photodegradation of RhB solution ( $1 \times 10^{-6}$  M) by  $\text{Ag}_3\text{PO}_4$  nanoparticles. Inset: correlation between the absorbance changes at absorption maximum (blue line) and the corresponding wavelength shifts (red line); (b) fluorescence spectral evolution of the RhB/ $\text{Ag}_3\text{PO}_4$  system under visible light irradiation. (c) Fluorescence decay curves (525–555 nm) of the RhB/ $\text{Ag}_3\text{PO}_4$  system in aqueous solution under different visible irradiation times. (d) Typical fluorescence lifetime of RhB (black line) and the intermediate deethylation products (red line) in aqueous solution.

Table 1 Dynamical parameters of photodegradation in RhB/ $\text{Ag}_3\text{PO}_4$  with irradiation time

Time (min)	1	5	9	15	28	45
( $\tau_1 = 1.75$ ns)	80%	55.4%	41.1%	33.1%	28.7%	19.5%
( $\tau_2 = 3.85$ ns)	20%	44.6%	58.9%	66.9%	71.3%	80.5%

In general, the RhB photodegradation consists of competitive or concomitant processes, namely the deethylation by photosensitization degradation and the destruction of the conjugated structure by photocatalytic processes.<sup>34</sup> For the latter case, the aromatic chromophore is attacked by the photogenerated active holes at the catalyst surface, leading to a direct decomposition of RhB without producing fluorescent intermediates. It has been proposed that electron transfer from the singlet excited state of the adsorbed dye to the CB of the semiconductor is the principal pathway to induce the initial step for producing deethylation from the RhB molecule.<sup>10</sup> In this situation, the strong interaction between the adsorbed dye and semiconductor surface is an important criterion for efficient electron or charge transfer. In the RhB/ $\text{Ag}_3\text{PO}_4$  system, we observed the deethylation of RhB from the above ensemble experiments, indicating an electron-injection process or a photosensitization process taking place from the singlet excited state of RhB to the CB of  $\text{Ag}_3\text{PO}_4$ . In the next section, we focus on the investigation to gain new insights into the

photosensitized degradation and the generation dynamics of the intermediates, especially at a single-molecule level.

### Photosensitization from ensemble to a single molecule

To observe the electron-injection process from RhB to  $\text{Ag}_3\text{PO}_4$  nanoparticles, we performed steady-state and time-resolved fluorescence measurements without visible light irradiation. As shown in Fig. 3a, the original RhB solution shows a strong fluorescence at 580 nm with the excitation of 488 nm, while the fluorescence intensity is remarkably decreased with the addition of  $\text{Ag}_3\text{PO}_4$  nanoparticles suspension into the RhB aqueous solution. This quenching effect is attributed to the electron transfer from the excited singlet state of RhB to the conduction band of the  $\text{Ag}_3\text{PO}_4$  nanoparticles,<sup>35</sup> constituting an electron-

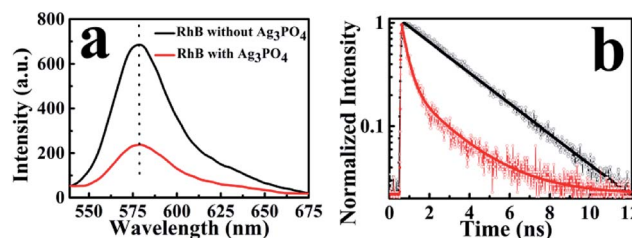


Fig. 3 (a) Emission spectra of RhB molecules with and without  $\text{Ag}_3\text{PO}_4$  nanoparticles in aqueous solution, (b) typical fluorescence decay curves of RhB molecules (black line) and RhB molecules on the  $\text{Ag}_3\text{PO}_4$  surface without water (red line).



injection process before the degradation of RhB molecule. This electron transfer was further confirmed by fluorescence lifetime measurements in the atmosphere. Two typical fluorescence decay traces of RhB molecules with and without  $\text{Ag}_3\text{PO}_4$  are shown in Fig. 3b. The decay curve of RhB molecules without  $\text{Ag}_3\text{PO}_4$  demonstrates a longer fluorescence lifetime. In contrast, the fluorescence lifetime of RhB molecules on the  $\text{Ag}_3\text{PO}_4$  surface is dramatically shortened, indicating the IET between RhB and  $\text{Ag}_3\text{PO}_4$  nanoparticles and confirming the rationality of the above-mentioned photosensitizing degradation. Usually, unconstrained bi-exponential and even multi-exponential fittings have to be considered to extract the decay components of adsorbed molecules on a catalyst surface with different active site distributions.<sup>36</sup>

To gain a new insight into this inhomogeneity, we performed single-molecule fluorescence lifetime measurements combined with confocal fluorescence microscopy to observe the behavior of a single RhB molecule on the  $\text{Ag}_3\text{PO}_4$  surface. Fig. 4a and b show the single-molecule fluorescence lifetime images of RhB on bare cover glass and on  $\text{Ag}_3\text{PO}_4$  nanoparticles-coated cover glass ( $20 \times 20 \mu\text{m}^2$ ,  $128 \times 128$  pixels matrix, 2 ms dwell time) under the same ambient conditions. The brightness and color of the light spot represent the fluorescence intensity and lifetime of a single molecule, respectively. Evidently, the

fluorescence lifetime of some RhB molecules on  $\text{Ag}_3\text{PO}_4$  particles-coated cover glass was shorter than that on bare cover glass, suggesting the occurrence of IET between these RhB molecules and the  $\text{Ag}_3\text{PO}_4$  nanoparticles. It should be mentioned that a brighter molecule can have a shorter lifetime or a long lifetime, and there is no direct relation between the fluorescence intensity and fluorescence lifetime.<sup>37</sup> Fig. 4c and d show the single-molecule fluorescence emission trajectories of RhB on the bare cover glass and on  $\text{Ag}_3\text{PO}_4$  particles surface (binning time, 10 ms), respectively. Compared to a nearly constant emission on the glass surface, the fluorescence intensity of RhB on  $\text{Ag}_3\text{PO}_4$  nanoparticle surface displays a strong fluctuation and blinking with the “dark” time ranging from sub-second to seconds, similar to the reports on  $\text{PF/TiO}_2$  (ref. 38) and  $\text{CdTe/PI-CA}$ .<sup>39</sup> With photoexcitation, the excited state of an individual molecule either undergoes radiative emission to yield a photon that contributes to a bright state or undergoes a non-radiative electron transfer process that contributes to the dark state.<sup>21</sup> In the fluorescence trajectory of RhB on  $\text{Ag}_3\text{PO}_4$  particles surface, the “bright” state mostly reflects a low IET activity associated with the radiative relaxation from an excited state to ground state. Correspondingly, the “dark” state with the intensity close to background level indicates a high IET efficiency, demonstrating a quenching effect of the fluorescence emission.

The interaction and surrounding microenvironment of each molecule on the  $\text{Ag}_3\text{PO}_4$  surface differs from time to time and from site to site, thus the lifetime distribution of RhB is supposed to be inhomogeneous as well. Fig. 4e displays two typical fluorescence decay traces of RhB molecules on bare cover glass and on  $\text{Ag}_3\text{PO}_4$  nanoparticles-coated cover glass. Both traces can be fitted with a single exponential decay with the average fluorescence lifetime of 3.45 ns and 1.85 ns for RhB and RhB/ $\text{Ag}_3\text{PO}_4$ , confirming the photosensitization through electron transfer from excited RhB to  $\text{Ag}_3\text{PO}_4$ . Fig. 4f shows the statistical analysis of the fluorescence lifetime distribution of single RhB molecule on bare cover glass and on  $\text{Ag}_3\text{PO}_4$  particles surface. We found a narrower distribution of fluorescence lifetime without  $\text{Ag}_3\text{PO}_4$  nanoparticles, ranging from 2.4 ns to 4.4 ns with a 0.6 ns full width at half maximum (FWHM). On the contrary, a wider distribution of fluorescence lifetimes ranging from 0.6 to 4.2 ns with a 1.4 ns FWHM was observed for RhB on the  $\text{Ag}_3\text{PO}_4$  nanoparticle surface. The average fluorescence lifetime ( $\sim 2.0$  ns) for RhB on the  $\text{Ag}_3\text{PO}_4$  particles surface was obviously smaller than that ( $\sim 3.5$  ns) for RhB on the glass surface, indicating a dye-sensitizing feature and electron injection from excited RhB to  $\text{Ag}_3\text{PO}_4$ , which is consistent with the observations in the ensemble experiments.

The broad lifetime distribution reflects different IET reactivity dynamics and the complexity of interactions and electronic coupling between RhB and  $\text{Ag}_3\text{PO}_4$  nanoparticles. To further confirm the heterogeneous photosensitizing in the RhB/ $\text{Ag}_3\text{PO}_4$  system, we recorded hundreds of emission trajectories of RhB molecules on  $\text{Ag}_3\text{PO}_4$  NPs-coated cover glass. Fig. 5 shows two typical single-molecule trajectories and their corresponding fluorescence decays. In the weak interaction case, the “bright” states of RhB emission dominate the intensity

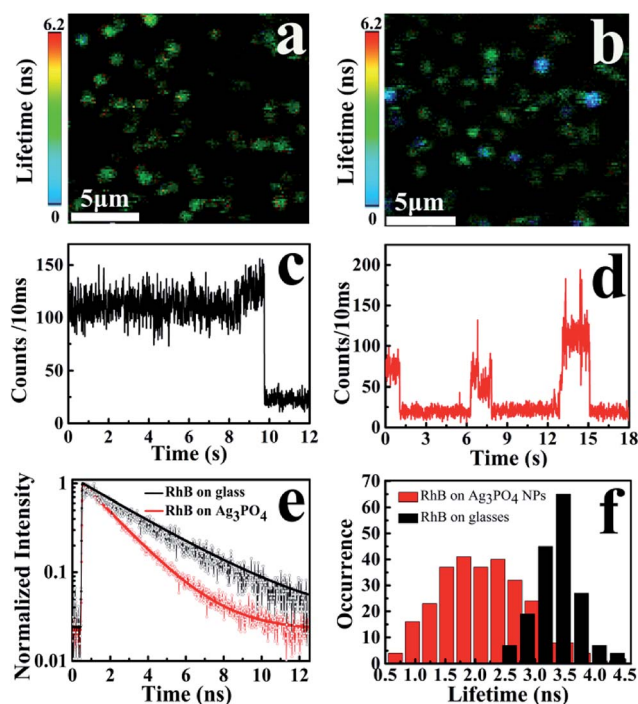


Fig. 4 Single-molecule fluorescence images of RhB on (a) bare cover glass and (b)  $\text{Ag}_3\text{PO}_4$  particles-coated cover glass (image size,  $20 \times 20 \mu\text{m}^2$ ) under the same fluorescence lifetime imaging conditions. (c, d) Typical fluorescence intensity trajectories of single-molecule RhB on (c) bare cover glass and (d)  $\text{Ag}_3\text{PO}_4$  particles-coated cover glass, with the binning time of 10 ms. (e) Typical fluorescence lifetime decay curves of RhB on bare cover glass (black line) and on  $\text{Ag}_3\text{PO}_4$  particles-coated cover (red line). (f) Single-molecule fluorescence lifetime distributions of RhB molecules on the bare cover glass (black) and on  $\text{Ag}_3\text{PO}_4$  particle surface (red).



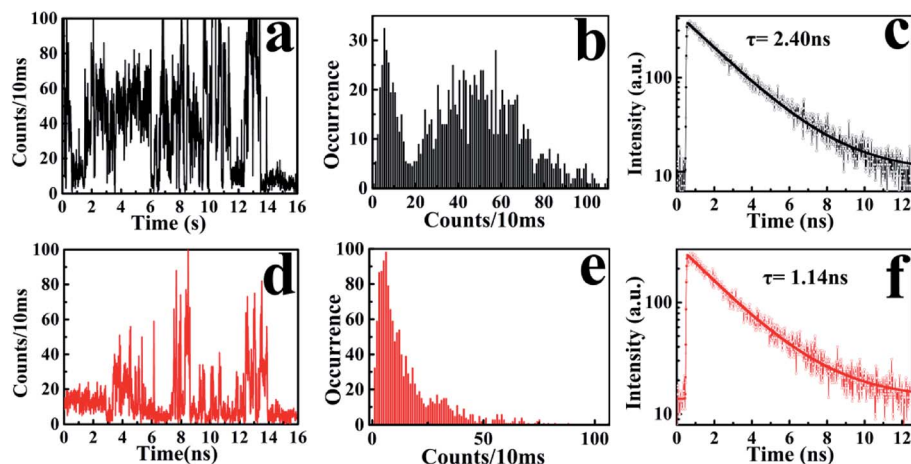


Fig. 5 (a) Bright and (d) dark states of single-molecule fluorescence intensity trajectories; (b) bright and (e) dark states of emission intensity histograms to determine the threshold for the bright and dark states in the RhB/Ag<sub>3</sub>PO<sub>4</sub> system, (c) bright and (f) dark states of the fluorescence lifetime decays.

trajectory, even though a certain amount of “dark” states can be observed (Fig. 5a). These molecules emit relatively more photons and exhibit a longer fluorescence lifetime before photobleaching or being degraded (Fig. 5b and c), and thus can be attributed to the physically adsorbed RhB molecules on the Ag<sub>3</sub>PO<sub>4</sub> surface. In contrast, the RhB molecule adsorbed on the active site of Ag<sub>3</sub>PO<sub>4</sub> nanoparticles has a higher IET efficiency and a shorter fluorescence lifetime (Fig. 5d and f), and emits a small amount of photons before being photobleached or photodegraded (Fig. 5e). Correspondingly, the intensity trajectory demonstrates a drastic fluctuation, where the “dark” states and “bright” states appear alternatively for this strong interaction case. The ratio between the radiative and non-radiative rates is primarily modulated by the interaction mode or strength with the catalyst surface. Therefore, we can infer that the photosensitizing activity is strongly related to the adsorption sites on the particle surface and the energetic coupling between the excited singlet state of RhB and the conduction band of a Ag<sub>3</sub>PO<sub>4</sub> nanoparticle. Similar single-molecule fluorescence behavior has been observed in other organic dye/semiconductor nanoparticle systems.<sup>20,21,38</sup> On the other hand, we can also speculate that the subsequent photodegradation of RhB by Ag<sub>3</sub>PO<sub>4</sub> nanoparticles is associated with the distribution of active sites on the Ag<sub>3</sub>PO<sub>4</sub> surface.

### Single-molecule observation of the photodegradation intermediates

According to the above-mentioned results and discussion, the photogenerated deethylation intermediate by Ag<sub>3</sub>PO<sub>4</sub> nanoparticles under visible irradiation shows a longer fluorescence lifetime compared with that of the RhB molecule in aqueous condition. Without visible irradiation, the RhB/Ag<sub>3</sub>PO<sub>4</sub> on the cover glass (without water) demonstrates a shorter fluorescence lifetime due to the injection electrons from RhB into the CB of the Ag<sub>3</sub>PO<sub>4</sub> semiconductor. Considering the co-existence of these features, we were inspired to observe the whole

photodegrading dynamics of a single RhB molecule on a Ag<sub>3</sub>PO<sub>4</sub> nanoparticle in aqueous conditions. Specifically, we expected to derive the precedence relation between the photosensitizing and photocatalytic degradation from the single-molecule emission fluctuation and lifetime sequencing with time, and to be able to correlate the degradation of RhB with the adsorbing sites on the Ag<sub>3</sub>PO<sub>4</sub> surface. As the generation of deethylation intermediate involves the formation of O<sub>2</sub><sup>•−</sup> radicals,<sup>11</sup> an aqueous atmosphere microenvironment for RhB/Ag<sub>3</sub>PO<sub>4</sub> was created before performing the single-molecule measurements. It should be mentioned that the excitation laser at 488 nm worked as the visible irradiation source to generate electron–hole pairs in the Ag<sub>3</sub>PO<sub>4</sub> nanoparticles, and also was used to excite the adsorbed RhB molecule and the

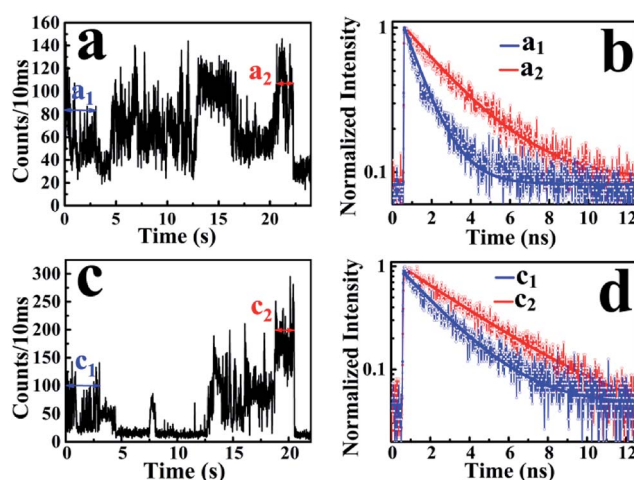


Fig. 6 Subsections of two representative single-molecule fluorescence trajectories and lifetime curves of RhB on Ag<sub>3</sub>PO<sub>4</sub>. (a) and (b) RhB adsorbed on the active site, where the time trace starts with a lifetime of 1.06 ns and ends with 2.80 ns. (c) and (d) Physically adsorbed RhB, where the time trace starts with a lifetime of 2.08 ns and ends with 3.09 ns.





intermediate deethylation of photocatalysis. Fig. 6a shows a representative single-molecule fluorescence time trajectory, which can be decomposed into two subintervals: the first half, section  $a_1$  and the second half, section  $a_2$ . At the beginning, the emission intensity level was around 60 counts/10 ms (section  $a_1$ ), while a higher level of about 120 counts/10 ms was observed before the end of photodegradation (section  $a_2$ ). From the time correlation analysis of photons in section  $a_1$ , a 1.06 ns fluorescence lifetime was obtained by mono-exponential fitting the decay curve (Fig. 6b), demonstrating an efficient photosensitization process. However, a longer fluorescence lifetime of 2.88 ns was acquired by analyzing the photons in section  $a_2$ , clearly indicating the formation of the deethylation intermediate. Similarly, Fig. 6c shows another representative single-molecule fluorescence trajectory and the derived lifetime traces from sections  $c_1$  and  $c_2$ . The intensity level was around 100 counts/10 ms and the lifetime was 2.08 ns in section  $c_1$ , while the corresponding values were 150 counts/10 ms and 3.09 ns in section  $c_2$ , respectively (Fig. 6d). Apparently, section  $a_1$  shows a shorter lifetime than section  $c_1$ , reflecting the efficient IET dynamics at the active sites on the  $\text{Ag}_3\text{PO}_4$  surface. For some single-molecule events, it was difficult to identify the discrete intensity-lifetime level in the emission trajectory, especially for the intensity fluctuation occurring on a time scale faster than the binning time, or where the intensity change is not large enough to be separated into discrete levels. Therefore, the most efficient photosensitization or IET process with a much shorter lifetime is hard to derive from the single trajectory of  $\text{RhB}/\text{Ag}_3\text{PO}_4$  in the aqueous microenvironment.

To confirm the extensive existence of photosensitized degradation and intermediate generation, we performed lifetime distribution analysis by monitoring hundreds of single-molecule emission trajectories. As shown in Fig. 7, there are two obviously separated lifetime distributions. The collected photons in the first half section demonstrate a broad lifetime distribution, consistent with the observations in single-molecule photosensitization, indicating different electron transfer efficiencies and

inhomogeneous interactions of RhB molecules with different adsorption sites on the  $\text{Ag}_3\text{PO}_4$  surface. In the tail section of the emission trajectory, the photons demonstrate a longer lifetime, reflecting the generation of the photocatalytic intermediate deethylation. These results clearly indicate that when the  $\text{Ag}_3\text{PO}_4$  photocatalyst and the adsorbed RhB molecule are excited by visible light at the same time, the photosensitization occurs prior to the photocatalytic degradation of RhB. Combining the results from the ensemble to a single molecule, we successfully observed the heterogeneous photosensitization and intermediate generation in the photocatalysis of the  $\text{RhB}/\text{Ag}_3\text{PO}_4$  system.

### Mechanism interpretation

Both photosensitization and photocatalysis in the  $\text{RhB}/\text{Ag}_3\text{PO}_4$  system can generate fluorescence quenching of adsorbed dye molecules, causing a simultaneous change in emission intensity and fluorescence lifetime but reflecting different interaction mechanisms. Under visible light irradiation, both  $\text{Ag}_3\text{PO}_4$  and RhB molecules can be excited in an aqueous environment. The electron in the singlet excited state of RhB is injected into the conduction band of  $\text{Ag}_3\text{PO}_4$ , where the IET efficiency depends on the interaction strength or the adsorption sites on the  $\text{Ag}_3\text{PO}_4$  surface. Therefore, the fluorescence lifetime of RhB is shortened compared to that without  $\text{Ag}_3\text{PO}_4$ , corresponding to the photosensitization process. This injected electron on  $\text{Ag}_3\text{PO}_4$  from the excited RhB can be captured by  $\text{O}_2$  to form  $\text{O}_2^{\cdot-}$ , which can attack the excited RhB molecule to generate the intermediate product with a longer lifetime. Meanwhile,  $\text{Ag}_3\text{PO}_4$  particle can also be excited to produce electron-hole pairs by visible light irradiation. In this case, the holes in the valence band of  $\text{Ag}_3\text{PO}_4$  can directly attack the adsorbed RhB molecule *via* the destruction of its conjugated structure, resulting in the photobleaching or complete degradation of RhB. In other words, electron injection is the principal pathway as an initiation step to observe the generation of the photochemical deethylation intermediate,<sup>10</sup> which has a blue-shifted emission spectrum and a longer fluorescence lifetime.

For clarity, the two competitive photodegradation processes, the so-called *N*-deethylation and chromophore cleavage, occur simultaneously in this  $\text{RhB}/\text{Ag}_3\text{PO}_4$  system under visible light irradiation and in aqueous environment, as illustrated in Fig. 8. For the chromophore cleavage case, the electron-hole pair in the  $\text{Ag}_3\text{PO}_4$  nanoparticle can be generated under visible light irradiation, that is, the electron is excited into the conduction band and a hole is left in the valence band. As one of most efficient reactive species in catalysis, this hole ( $h^+$ ) can directly attack and oxidize the adsorbed RhB on the surface of the  $\text{Ag}_3\text{PO}_4$  nanoparticle, leading to the photodegradation of RhB through the destruction of its conjugated structure.<sup>27,40</sup> In this case, the product of the photocatalytic degradation was not observed in our single molecule fluorescence measurements, even though the ensemble fluorescence quenching partially came from this degradation contribution. In particular, this hole-oxidizing photodegradation plays a major role in non-aqueous environments, and it is not surprising to observe a shorter emission duration time in the single-molecule photosensitizing measurement. In

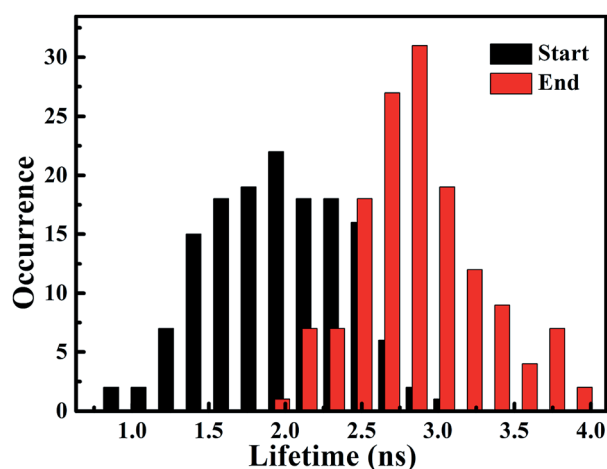


Fig. 7 Distribution histogram of single molecule fluorescence lifetime derived from start section (black column) and end section (red column) of intensity trajectories.



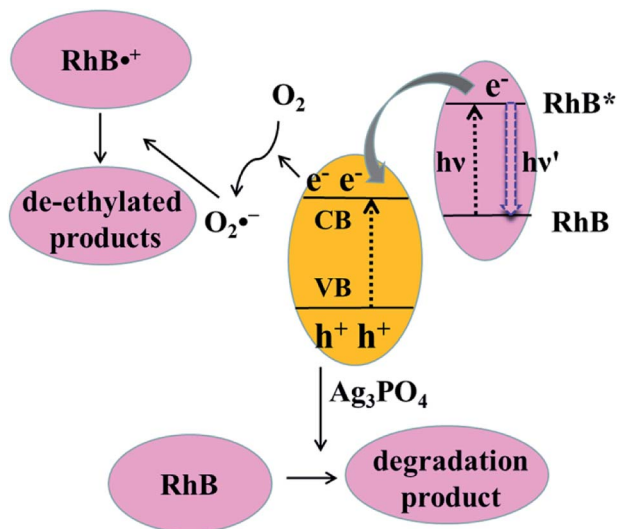


Fig. 8 Photodegradation diagram of RhB molecules on the surface of the  $\text{Ag}_3\text{PO}_4$  nanocatalyst.

principle, the photogenerated active species, such as  $\text{OH}^\bullet$  radicals, could also directly attack the central carbon of the RhB molecule to some extent. However, a previous study indicated that the  $\text{OH}^\bullet$  radical scavenger has no observable effect on the photodegradation rate of RhB in the  $\text{Ag}_3\text{PO}_4$  system.<sup>41</sup> Thus, the contribution from  $\text{OH}^\bullet$  radicals could be negligible in this work. Since the absorption cross-section of  $\text{Ag}_3\text{PO}_4$  nanoparticles is much smaller than that of RhB molecules at the excitation wavelength, the photosensitization process prior to degradation plays an important role in this RhB/ $\text{Ag}_3\text{PO}_4$  model system. When the adsorbed RhB molecule is excited from the ground state ( $S_0$ ) to the excited state ( $S_1$ ) by visible light, the electron will be injected into the CB of  $\text{Ag}_3\text{PO}_4$  catalyst, with the inhomogeneous efficiency associated with the adsorption sites and interaction strength. This photosensitized interfacial electron transfer will generate a temporal  $\text{RhB}^{\bullet+}$  before recombining with an electron. In the meantime, the  $\text{O}_2$  molecule around the  $\text{Ag}_3\text{PO}_4$  catalyst surface in the aqueous environment can be reduced by the transferred electron or photogenerated electron-hole pair in  $\text{Ag}_3\text{PO}_4$  to form  $\text{O}_2^{\bullet-}$  radicals, which is a critical step in the photosensitized degradation of RhB molecules. Once the active  $\text{O}_2^{\bullet-}$  radical is created, the temporal  $\text{RhB}^{\bullet+}$  generated after electron injection into  $\text{Ag}_3\text{PO}_4$  will be attacked to produce *N*-deethylation intermediates, rather than to attack the conjugated structure in the oxygen-rich aqueous atmosphere.<sup>11</sup> These deethylation intermediates will be degraded completely by the surrounding radicals. Therefore, an important photodegradation pathway of RhB by  $\text{Ag}_3\text{PO}_4$  nanoparticles in aqueous environment consists of a pre-photosensitization process and the intermediate generation of *N*-deethylation, which demonstrates a clear inhomogeneity and dynamical characteristics.

## Conclusions

We systematically investigated the inhomogeneous interactions between the dye molecule RhB and semiconductor  $\text{Ag}_3\text{PO}_4$

nanoparticle, as well as the intermediates generation in the photodegradation process, by using ensemble-averaged spectroscopy and single-molecule, single-particle FLIM spectroscopy. The as-prepared  $\text{Ag}_3\text{PO}_4$  nanoparticles demonstrated good catalytic activity under visible light irradiation in aqueous environment. Besides the direct oxidation of RhB by photo-generated holes in  $\text{Ag}_3\text{PO}_4$  nanoparticles, the degradation process *via* intermediate generation plays an important role in the photodegradation. The intermediate product deethylation has a blue-shifted absorption and fluorescence bands, and a longer fluorescence lifetime compared with that of RhB molecules in aqueous solution. The fluorescence quenching and lifetime shortening of a RhB molecule on the  $\text{Ag}_3\text{PO}_4$  surface suggest photosensitization in the RhB/ $\text{Ag}_3\text{PO}_4$  system prior to the photodegradation of the RhB molecule.

The photosensitized photodegradation process of RhB on the  $\text{Ag}_3\text{PO}_4$  nanoparticle surface was successfully characterized by analyzing the single-molecule fluorescence intensity fluctuation and lifetime distribution. The single-molecule fluorescence intensity fluctuations of RhB were closely associated with the photosensitization activities and IET efficiencies. The dominant dark states in the fluorescence intensity trajectory with a shorter lifetime demonstrate a higher charge injection process taking place at the active sites. The observed broad distribution of the single-molecules lifetimes reflects the heterogeneous interactions between RhB molecules and  $\text{Ag}_3\text{PO}_4$  nanoparticles, correlated to the distribution of active sites on the  $\text{Ag}_3\text{PO}_4$  nanoparticles. The shorter fluorescence lifetime derived from the starting subsection than that from the end subsection of a single-molecule intensity trajectory clearly reveals the photosensitized photodegradation of RhB and the intermediate generation in the aqueous environment. Moreover, this time dependency of the subsection fluorescence lifetime indicates that the electron injection from the adsorbates to catalyst occurs prior to radical attack in photosensitized degradation. These findings at a single-molecule level provide new insights into understanding the inhomogeneous photosensitization and photodegradation processes involved in solar energy conversion and photocatalysis.

## Conflicts of interest

There are no conflicts of interest to declare.

## Acknowledgements

The work was financially supported by the National Science Foundation Committee of China (Project No. U1604129, U1404619, U1504510 and 21173068) and Natural Science Foundation of Henan Province 162300410028.

## Notes and references

- 1 J. Romao and G. Mul, *ACS Catal.*, 2016, **6**, 1254–1262.
- 2 Y. Lin, D. Li, J. Hu, G. Xiao, J. Wang, W. Li and X. Fu, *J. Phys. Chem. C*, 2012, **116**, 5764–5772.





- 3 M. T. Uddin, Y. Nicolas, C. Olivier, T. Toupance, L. Servant, M. M. Mueller, H.-J. Kleebe, J. Ziegler and W. Jaegermann, *Inorg. Chem.*, 2012, **51**, 7764–7773.
- 4 A. Mukherji, B. Seger, G. Q. Lu and L. Wang, *ACS Nano*, 2011, **5**, 3483–3492.
- 5 Y.-S. Chen and P. V. Kamat, *J. Am. Chem. Soc.*, 2014, **136**, 6075–6082.
- 6 J. Liu, Y. Zhao, L. Shi, S. Yuan, J. Fang, Z. Wang and M. Zhang, *ACS Appl. Mater. Interfaces*, 2011, **3**, 1261–1268.
- 7 S. Ardo, D. Achey, A. J. Morris, M. Abrahamsson and G. J. Meyer, *J. Am. Chem. Soc.*, 2011, **133**, 16572–16580.
- 8 S. Balasubramanian, P. Wang, R. D. Schaller, T. Rajh and E. A. Rozhkova, *Nano Lett.*, 2013, **13**, 3365–3371.
- 9 S. E. Koops, B. C. O'Regan, P. R. F. Barnes and J. R. Durrant, *J. Am. Chem. Soc.*, 2009, **131**, 4808–4818.
- 10 J. Zhuang, W. Dai, Q. Tian, Z. Li, L. Xie, J. Wang, P. Liu, X. Shi and D. Wang, *Langmuir*, 2010, **26**, 9686–9694.
- 11 H. Fu, S. Zhang, T. Xu, Y. Zhu and J. Chen, *Environ. Sci. Technol.*, 2008, **42**, 2085–2091.
- 12 J. B. Asbury, E. Hao, Y. Q. Wang, H. N. Ghosh and T. Q. Lian, *J. Phys. Chem. B*, 2001, **105**, 4545–4557.
- 13 D. A. Gaal and J. T. Hupp, *J. Am. Chem. Soc.*, 2000, **122**, 10956–10963.
- 14 V. Biju, M. Micic, D. H. Hu and H. P. Lu, *J. Am. Chem. Soc.*, 2004, **126**, 9374–9381.
- 15 M. B. J. Roeflaers, B. F. Sels, H. Uji-i, F. C. De Schryver, P. A. Jacobs, D. E. De Vos and J. Hofkens, *Nature*, 2006, **439**, 572–575.
- 16 P. C. Sevinc, X. Wang, Y. Wang, D. Zhang, A. J. Meixner and H. P. Lu, *Nano Lett.*, 2011, **11**, 1490–1494.
- 17 Y. Park, W. Kim, D. Monllor-Satoca, T. Tachikawa, T. Majima and W. Choi, *J. Phys. Chem. Lett.*, 2013, **4**, 189–194.
- 18 J. Li, I. Kondov, H. Wang and M. Thoss, *J. Phys. Chem. C*, 2010, **114**, 18481–18493.
- 19 T. Tachikawa, S. Yamashita and T. Majima, *J. Am. Chem. Soc.*, 2011, **133**, 7197–7204.
- 20 Y. Wang, X. Wang, S. K. Ghosh and H. P. Lu, *J. Am. Chem. Soc.*, 2009, **131**, 1479–1487.
- 21 V. G. Rao, B. Dhital, Y. He and H. P. Lu, *J. Phys. Chem. C*, 2014, **118**, 20209–20221.
- 22 L. Damalakiene, V. Karabanovas, S. Bagdonas and R. Rotomskis, *Int. J. Mol. Sci.*, 2016, **17**, 473.
- 23 L. Zhang, J. Lei, J. Liu, F. Ma and H. Ju, *Biomaterials*, 2015, **67**, 323–334.
- 24 K. Okabe, N. Inada, C. Gota, Y. Harada, T. Funatsu and S. Uchiyama, *Nat. Commun.*, 2012, **3**, 705.
- 25 A. Orte, J. M. Alvarez-Pez and M. J. Ruedas-Rama, *ACS Nano*, 2013, **7**, 6387–6395.
- 26 Z. Yi, J. Ye, N. Kikugawa, T. Kako, S. Ouyang, H. Stuart-Williams, H. Yang, J. Cao, W. Luo and Z. Li, *Nat. Mater.*, 2010, **9**, 559–564.
- 27 M. Ge, *Chin. J. Catal.*, 2014, **35**, 1410–1417.
- 28 Y. Bi, S. Ouyang, N. Umezawa, J. Cao and J. Ye, *J. Am. Chem. Soc.*, 2011, **133**, 6490–6492.
- 29 L. Wang, J. Shang, W. Hao, S. Jiang, S. Huang, T. Wang, Z. Sun, Y. Du, S. Dou, T. Xie, D. Wang and J. Wang, *Sci. Rep.*, 2014, **4**, 7384.
- 30 K. Yu, S. G. Yang, H. He, C. Sun, C. G. Gu and Y. M. Ju, *J. Phys. Chem. A*, 2009, **113**, 10024–10032.
- 31 C. C. Chen, W. Zhao, J. Y. Li and J. C. Zhao, *Environ. Sci. Technol.*, 2002, **36**, 3604–3611.
- 32 Z.-R. Tang, Y. Zhang, N. Zhang and Y.-J. Xu, *Nanoscale*, 2015, **7**, 7030–7034.
- 33 Z. Xiong, L. L. Zhang, J. Ma and X. S. Zhao, *Chem. Commun.*, 2010, **46**, 6099–6101.
- 34 T. Wu, G. Liu, J. Zhao, H. Hidaka and N. Serpone, *J. Phys. Chem. B*, 1998, **102**, 5845–5851.
- 35 A.-H. Liang, S.-M. Zhou and Z.-L. Jiang, *Talanta*, 2006, **70**, 444–448.
- 36 S. Saraswat, A. Desireddy, D. Zheng, L. Guo, H. P. Lu, T. P. Bigioni and D. Isailovic, *J. Phys. Chem. C*, 2011, **115**, 17587–17593.
- 37 Y. He, V. G. Rao, J. Cao and H. P. Lu, *J. Phys. Chem. Lett.*, 2016, **7**, 2221–2227.
- 38 L. Guo, Y. Wang and H. P. Lu, *J. Am. Chem. Soc.*, 2010, **132**, 1999–2004.
- 39 S.-C. Cui, T. Tachikawa, M. Fujitsuka and T. Majima, *J. Phys. Chem. C*, 2008, **112**, 19625–19634.
- 40 W. Teng, X. Li, Q. Zhao, J. Zhao and D. Zhang, *Appl. Catal., B*, 2012, **125**, 538–545.
- 41 M. Ge, N. Zhu, Y. Zhao, J. Li and L. Liu, *Ind. Eng. Chem. Res.*, 2012, **51**, 5167–5173.

